Structure and Mechanism of Human DNA Polymerase η

Christian Biertümpfel[1], **Ye Zhao**[2,1], **Yuji Kondo**[3], **Santiago Ramón-Maiques**[1,6], **Mark Gregory**[1], **Jae Young Lee**[1,7], **Chikahide Masutani**[3], **Alan R. Lehmann**[5], **Fumio Hanaoka**[3,4], and **Wei Yang**[1]

[1]Laboratory of Molecular Biology, NIDDK, NIH

[2]Institute of Nuclear-Agricultural Sciences, Zhejiang University, China

[3]Graduate School of Frontier Biosciences, Osaka University, Japan

[4]Faculty of Science, Gakushuin University, Tokyo, Japan

[5]Genome Damage and Stability Centre, University of Sussex, Brighton, UK

Abstract

The variant form of human xeroderma pigmentosum syndrome (XPV) is caused by a deficiency in DNA polymerase η (Pol η) that enables replication through sunlight-induced pyrimidine dimers. We report high-resolution crystal structures of human Pol η at four consecutive steps during DNA synthesis through *cis-syn* cyclobutane thymine dimers. Pol η acts like a molecular splint to stabilize damaged DNA in a normal B-form conformation. An enlarged active site accommodates the thymine dimer with excellent stereochemistry for two-metal ion catalysis. Two residues conserved among Pol η orthologs form specific hydrogen bonds with the lesion and the incoming nucleotide to assist translesion synthesis. Based on the structures, eight Pol η missense mutations causing XPV can be rationalized as undermining the "molecular splint" or perturbing the active-site alignment. The structures also shed light on the role of Pol η in replicating through D loop and DNA fragile sites.

Wei Yang Wei.Yang@nih.gov, LMB, NIDDK, NIH, 9000 Rockville Pike, Bldg. 5, Rm B1-03, Bethesda, MD 20892. phone: (301) 402-4645, fax: (301) 496-0201, Fumio Hanaoka fumio.hanaoka@gakushuin.ac.jp, Faculty of Science, Gakushuin University, 1-5-1 Mejiro, Toshima-ku, Tokyo 171-8588, Japan, phone: +81-3-3986-0221 ex. 6457, fax: +81-3-5992-1029.
[6]Current address, Spanish National Cancer Research Centre, Madrid, Spain
[7]Current address, Dongguk University-Seoul, Seoul, Korea

Introduction

Life on earth can scarcely escape the ultraviolet radiation (UV) of sunlight, which catalyzes covalent linkages between adjacent pyrimidines in DNA1. The resulting pyrimidine dimers are roadblocks to most DNA polymerases, but the human *POLH* gene, defective in the variant form of xeroderma pigmentosum (XPV), encodes a Y-family DNA polymerase, Pol η, specialized for translesion synthesis (TLS) through cyclobutane pyrimidine dimers (CPDs)2,3. XPV is characterized by sunlight-induced pigmentation changes and a highly elevated incidence of skin malignancies. In contrast to humans, yeast lives well without Pol η when chronically exposed to a low dosage of UV radiation4. Conversely, in humans TLS by Pol η can decrease cellular sensitivity to anticancer DNA adducts, e.g. cisplatin5. In addition to TLS, Pol η is involved in somatic hypermutation6 and replication of D loop and DNA fragile sites7–10.

Pol η is the only one of the fifteen human DNA polymerases in which defects are unequivocally associated with cancer11–13. Among human Y-family polymerases (Rev1, Pols η,ι and κ), the lesion-bypass specificity and efficiency of Pol η stand out. Pol η binds CPD-containing DNA better than undamaged DNA and extends primers more processively opposite and up to 2 nt beyond CPDs14,15. Yet Pol η is completely blocked by UV-induced pyrimidine (6-4) pyrimidone photoproducts (6-4PP)16. 6-4PPs occur less frequently than CPDs and distort the helical structure of DNA more severely and are thus more efficiently recognized and removed by nucleotide-excision repair proteins17,18.

Structural analyses of these TLS polymerases reveal a spacious active site that accommodates DNA adducts and non-Watson-Crick base pairs with little discrimination19,20. However, the molecular basis for the specificity and efficiency of Pol η in DNA synthesis through CPDs has remained a puzzle despite many crystal structures, including those of the apo and cisplatin-DNA bound yeast Pol η21,22.

We report here crystal structures of the polymerase domain of human Pol η catalyzing the four-step TLS through a cis-syn thymine dimer and in a ternary complex with a normal DNA. Complementing these structures, two residues conserved among Pol η orthologs were mutated, and the resulting defects in TLS assessed by functional studies.

Crystallization and features of hPol η

The catalytic domain of human Pol η (1–432 aa) (abbreviated as hPol η) was expressed in *E. coli* after codon optimization (Methods). Crystals of ternary complexes were initially grown with normal DNAs, and the structure was solved and refined to 2.9Å resolution. However, a hydrophobic crystal-lattice contact between protein molecules appeared to distort hPol η-DNA interactions as compared with known structures of Y-family polymerases (Supplementary Fig. 1). Multiple amino-acid substitutions were engineered to break this lattice contact. Non-hydrolyzable dNMPNPPs were synthesized to replace dNTPs for co-crystallization of an active hPol η, DNA and Mg^{2+}. Different DNA lengths were systematically sampled and proven most effective for breaking the undesirable lattice contacts. After many trials, two new crystal forms were grown that diffracted X-rays to ~3Å and subsequently improved to 1.75 to 2.15Å (Supplementary Table 1–2).

The crystal structure of WT hPol η complexed with normal DNA and dAMPNPP opposite the template T (denoted Nrm) was determined and refined to 1.83Å (Methods) (Fig. 1a). The relevance of the structure is validated by the appearance of a well-formed active site centered on two properly coordinated Mg^{2+} ions and the 3′-OH of the primer strand 3.2Å from the α-phosphate of dAMPNPP poised for in-line nucleophilic attack (Fig. 1b). The single water ligand of the Mg^{2+} ions (Fig. 1b) has been observed in several DNA polymerases and may participate in catalysis[23]. Configured around the non-hydrolyzable dNTP analog, the active site is arguably the most reaction ready among the homologous A-, B- and Y-family DNA polymerases crystallized to date. The incoming nucleotide, catalytic carboxylates and metal ions are nearly superimposable with those of human Pol β (X-family) despite dissimilar tertiary structures (Supplementary Fig. 2). This active site configuration is likely conserved among all DNA polymerases and possibly all RNA polymerases as well.

Like all Y-family polymerases, hPol η contains four domains—palm, finger, thumb and little finger (LF)—with the active site in the palm domain and DNA bound between thumb and LF. Unlike the structures of yeast Pol η–cisplatin complexes[22], hPol η's finger is closed and contacts the replicating base pair (Fig. 1c, Supplementary Fig. 3a), and LF interacts extensively with both template and primer in the major groove (Fig. 1d). A surface area of 2200Å^2 is buried between hPol η and DNA. The finger, palm and incoming dNTP in hPol η superimpose well with those in Dpo4 and Pols κ and ι (Supplementary Fig. 3a). Uniquely in hPol η, however, two bases of the template strand instead of one are in the active site, and the 3′ T is base paired with the incoming dAMPNPP (Fig. 1c). Translocation of two template bases into the active site was previously observed with Dpo4, but there the 5′ base was paired with the dNTP resulting in a misalignment[24]. In hPol η a slight shift of LF relative to the finger domain enlarges the active site, and allows it to accommodate two template bases without misalignment. Concomitantly, hPol η's thumb and LF are oriented differently relative to Dpo4 and Pols κ and ι (Supplementary Fig 3a). The thumb domain only contacts the DNA primer (Fig. 1d).

Structures displaying TLS through a CPD

CPD-containing oligonucleotides were synthesized to place each crosslinked thymine at the template position or 1 or 2 bp upstream (Supplementary Table 1). Four ternary complexes were crystallized and labeled as TT1, TT2, TT3 and TT4. All except TT2 were crystallized in the same space group as the complex of normal DNA (Nrm). These structures were determined by molecular replacement (Methods). After refinement, the four CPD-containing complexes are virtually superimposable with Nrm (Fig. 2a). The rmsds among proteins are 0.15 to 0.71Å over ~400 pairs of Cα atoms.

In TT1 the 3′ thymine of CPD serves as the template and forms a Watson-Crick (WC) base pair with dAMPNPP, much like an undamaged base (Fig. 2b). The 5′ thymine of CPD is turned and moved closer to the finger domain than the undamaged base in Nrm. The tighter interactions with the CPD may explain the better fidelity of hPol η in TLS (Fig. 3a). S62 forms van der Waals contacts with the 5′ base in both cases (Fig. 1c), but S62 is not conserved and replacing it with Gly increases the TLS efficiency of hPol η[25]. Even with the

S62G substitution, a 6-4PP would not fit in the active site (Supplementary Fig. 4a), which explains the selectivity of Pol η.

In TT2, the 5′ thymine of CPD also forms a WC base pair with dAMPNPP (Fig. 2c). The finger domain in TT2 is more open than in the other hPol η complex structures. Despite being crosslinked and rotationally constrained (Fig. 2a), the 3′ thymine of the CPD maintains a WC basepair with the primer, which undergoes minimal changes relative to the Nrm and TT1 complexes. This differs from CPDs complexed with a stalled replicative polymerase, where only one crosslinked thymine is base paired[26]. In TT1 and TT2, the template thymine adopts the position most similar to that of undamaged DNA, and the crosslinked partners adjust. In TT2 the deoxyribose of the 3′ thymine moves by 2–3Å and the base is shifted toward the major groove by ~2Å and tilted by ~20° (Fig. 2c).

Each template thymine in TT1 and TT2 is hydrogen bonded to Q38 of hPol η via its O2 oxygen (Fig. 2b–c). Both cytosine and thymine are vulnerable to forming UV-induced CPDs, and both have the O2 to form the hydrogen bond with Q38 as observed in TT1 to TT4 (Fig. 2d). In Nrm Q38 is instead hydrogen bonded with deoxyribose (Fig. 2b) due to a slight shift of the DNA template (Fig. 2a). Q38 is one of the two residues uniquely conserved in the Pol η family (Supplementary Fig. 5). Ala substitution of Q38 reduces the catalytic efficiency as expected (Fig. 3a). Interestingly, Q38A increases polymerase stalling after the CPD at the stage equivalent to TT3 (Fig. 3b). This stalling likely occurs because the template base cannot stack with the upstream CPD (Fig. 2e) and depends on Q38, its sole contact with the polymerase, to align with the incoming dNTP.

The second invariant residue in the Pol η family is an Arg (R61 in hPol η). In the yeast Pol η-cisplatin DNA complex crystal structures, its equivalent (R73) forms cation-π interactions with the base and polar interactions with the phosphates of the incoming dNTP[22]. In the five hPol η structures, the closed finger domain prevents R61 from stacking with the base. R61 instead adopts different rotamer conformations and is hydrogen bonded with the N7 of purines (A or G) or the phosphates (Fig. 2b–d), thus favoring the anti-conformation of dNTP and preventing Hoogsteen base pairing[27]. Ala substitution of R61 reduces the polymerase efficiency as well as misincorporation of dG opposite a template T (Fig. 3a). However, dGTP would be the correct incoming nucleotide if a cytosine is in the CPD. R61 is thus important for Pol η to efficiently synthesize DNA through cis-syn cytosine and thymine dimers but at the cost of potential misincorporation.

hPol η is a molecular splint

The DNAs in all four CPD-Pol η complexes maintain a straight B-form conformation (Fig. 2a) in spite of the inability of CPDs to base stack. This unperturbed structure is a stark contrast to the bent and unwound structures of CPD-containing DNAs alone or complexed with repair proteins (Supplementary Fig. 6)[28–31]. Poor base stacking and segmentation of the DNA helices are the structural features of CPDs that are recognized by repair proteins[32]. However, when complexed with hPol η, lesion-induced perturbations are absorbed by minor adjustments to torsion-angles of the surrounding nucleotides.

hPol η acts like a molecular splint to keep the damaged DNA straight and rigid owing to a continuous and highly positively charged DNA-binding surface that interacts extensively with the four template nucleotides immediately upstream of the active site (Fig. 4a). A β strand in LF (aa 316 to 324) is nearly parallel to the template strand, and every other mainchain amide donates a hydrogen bond to the template phosphates (Fig. 1d, 4b). Each phosphate forms additional hydrogen bonds with sidechains of Arg, Lys, Tyr and Thr. In contrast, the template-binding surface in other Y-family polymerases has a gap or holes owing to separations between LF and the catalytic core (palm, thumb and finger) (Fig. 4a, Supplementary Fig. 3a). The gap is particularly large in Pol κ, and the divided protein requires an N-terminal appendage (N-clasp) for stabilization[33]. Pol κ and Dpo4 likely use the structural gaps (Fig. 4a) to accommodate bulky minor-groove adducts during TLS[34,35]. The gaps in Dpo4 and Dbh also promote template looping out as a means of lesion bypass[36,37]. In hPol η LF is connected to the catalytic core by hydrogen bonds, salt bridges and hydrophobic interactions (Supplementary Fig. 3b–c). The resulting DNA-binding surface constrains the template backbone and reinforces a B-form structure in spite of CPDs.

The sidechains of R93 and R111 extend from the palm domain to the template strand and further strengthen this molecular splint. R93 connects the template strand with the incoming nucleotide via its neighbor Y92, which stacks with F18 (the steric gate)[38] and the deoxyribose of dNTP (Fig. 1c). Although this Y92/R93 pair is found in Pols ι and κ, only in Pol η is the DNA template hydrogen bonded to R93. R111 is adjacent to the catalytic carboxylate D115 and interacts with both LF and the template strand (Fig. 5a), which explains why substitution of R111 by His leads to the XPV phenotype[11].

Dissociation of hPol η after CPDs

TLS polymerases are recruited to stalled replication forks by Rad6-Rad18 mediated ubiquitination of PCNA[39]. Dissociation following TLS, however, may be an intrinsic property of human Pol η because of reduced affinity for DNA 3 bp past the CPD[14,15]. In all five structures, the DNA-binding surface of hPol η makes extensive interactions with 4 bp (Fig. 4), but has reduced interactions with the template strand further upstream. Modeling a CPD 1bp further upstream from TT4 reveals steric clashes of its phosphates with hPol η in addition to the loss of favorable hydrogen bonds (Supplementary Fig. 4b).

The crosslinked thymines are shifted 1–2Å into the major groove (Fig. 2). The C5 methyl groups form van der Waals contacts with LF (L378 and F423) in TT3 and TT4 (Fig. 4c). In Nrm, the space between the DNA bases and LF is filled with water and glycerol molecules. These major-groove interactions are lost when the CPD is 3 bp beyond the active site. The position-dependent CPD-Pol η interactions provide a structural basis for polymerase switching after lesion bypass.

XPV mutations and beyond

Many mutations in Pol η have been identified in XPV patients, and five missense mutations R111H, A117P, T122P, G263V and R361S are within the first 432 aa[11,12]. These mutations and three newly identified XPV mutations (A264P, F290S and G295R; ARL, unpublished data) are modeled in Fig. 5b. A117 adjoins the catalytic carboxylate E116, and

substitution by Pro would cause clashes with the carbonyl oxygen of V12. T122 occurs at the beginning of an α-helix and participates in the hydrogen-bond network surrounding all three catalytic carboxylates (D13, D115 and E116) (Fig. 5c). T122P would likely perturb the active site as does A117P. R111 is a part of the molecular splint (see the previous section). R361 is hydrogen bonded with the carbonyl oxygen of P316 and anchors the β strand (aa 316–324) for template binding (Fig. 5a,d). The R111H and R361S mutations are likely to relax the protein-DNA interface and break the molecular splint.

The remaining four XPV mutations are in the thumb domain and affect primer binding, which is essential to complete the molecular splint. G263 to Val and A264 to Pro mutations would cause steric clashes with the carbonyl oxygens of L258 and K261, respectively (Fig. 5e). These clashes would disrupt primer binding by the GGK motif (259–261aa) (Fig. 1d, 4c). F290 and G295 form the hydrophobic core of the thumb domain, and F290S and G295R mutations would destabilize the structure. Homozygous W174C has been implicated in XPV13, and V99M and I272T have been found in melanoma patients40. However, they are unlikely to directly alter the structure or polymerase activity of Pol η (Supplementary Fig. 7).

hPol η has been shown to synthesize through D loop and fragile sites, which contain hairpins and non-B-form structures7–10. Interestingly, in both crystal forms of hPol η the back of LF interacts with a neighboring DNA (Supplementary Fig. 8). The two symmetry-related DNA molecules are reminiscent of D-loop and hairpin structures as the template strands are nearly contiguous. Mimics of downstream DNA have not been observed previously in polymerase-DNA co-crystals. Many Pol η appear to retain the backside DNA-binding potential although the interfacial residues (R81, R84 and W339) are not strictly conserved (Supplementary Fig. 5). We hypothesize that the back of hPol η may be an authentic downstream DNA-binding site, and the LF serves as a wedge to separate non-B-form DNAs and aids the molecular splint to complete replication through D loop and fragile sites.

Concluding remarks

Human Pol η is specifically optimized for bypassing the most ubiquitous DNA lesion. An enlarged active site accommodates CPDs, the complementary DNA-binding surface reinforces the B-form conformation, and hydrophobic residues interact with crosslinked pyrimidines in the major groove. These features readily explain the specificity of human Pol η in TLS through CPDs and reduced efficiencies for other lesions including cisplatin 41–44. The limited interactions with the DNA minor groove may enable Pol η to misincorporate nucleotides during somatic hypermutation. The high-resolution structures reported here not only provide a detailed mechanism of TLS but also generate testable models for investigating novel functions of Pol η.

METHODS

The full-length human Pol η gene codon-optimized for *E. coli* expression was synthesized by GenScript. The catalytic core (aa 1–432, hPol η) was cloned into modified pET28a45, expressed in *E. coli* and purified by Ni^{2+}-affinity, MonoS and Superdex75 chromatography.

The His-tag was removed by PreScission protease. Mutagenesis was performed using QuikChange (Stratagene). Non-hydrolyzable dNMPNPPs were purchased from Jena Bioscience, and phosphoramidites of CPD from Glen Research. CPD oligos were synthesized and purified by TriLink Biotechnogies. Ternary complexes were prepared by mixing WT or C406M mutant hPol η and annealed DNA at a 1:1.05 molar ratio and addition of 5 mM Mg^{2+} and 1 mM non-hydrolyzable deoxynucleotides (dNMPNPP). The final protein concentration was 6–7 mg/ml. Crystals were grown in 0.1 M MES (pH 6.0), 19–21% (w/v) PEG 2K-MME and 5 mM $MgCl_2$ after several rounds of microseeding. Diffraction data were collected at sectors 22 and 23 of the APS. Phases were determined by molecular replacement[46] and multi-wavelength anomalous dispersion using selenomethionine-labeled hPol η[47]. Structures were refined using CNS[48] and interspersed with manual model building using COOT[49]. All residues are in the most favorable (97%) and allowed (2.3%) regions of Ramachandran plot except for two that are well defined by electron densities. For functional assays, the C-terminal truncated human Pol η (1–511aa), which has the same TLS activity as the full-length hPol η[43], was subcloned into pET21a and readily expressed in *E. coli*. Q38A and R61A mutations were made using Mutant-K (TaKaRa BIO Inc). Steady-state kinetic assays and primer extension reactions were carried out as described[43].

Supplementary Material

Refer to Web version on PubMed Central for supplementary material.

Acknowledgment

References

1. Brash DE. Sunlight and the onset of skin cancer. Trends Genet. 1997; 13:410–414. [PubMed: 9351343]

2. Masutani C, et al. The XPV (xeroderma pigmentosum variant) gene encodes human DNA polymerase η. Nature. 1999; 399:700–704. [PubMed: 10385124]

3. Johnson RE, Kondratick CM, Prakash S, Prakash L. hRAD30 mutations in the variant form of xeroderma pigmentosum. Science. 1999; 285:263–265. [PubMed: 10398605]

4. Hishida T, Kubota Y, Carr AM, Iwasaki H. RAD6-RAD18-RAD5-pathway-dependent tolerance to chronic low-dose ultraviolet light. Nature. 2009; 457:612–615. [PubMed: 19079240]

5. Chaney SG, Campbell SL, Bassett E, Wu Y. Recognition and processing of cisplatin- and oxaliplatin-DNA adducts. Crit Rev Oncol Hematol. 2005; 53:3–11. [PubMed: 15607931]

6. Saribasak H, Rajagopal D, Maul RW, Gearhart PJ. Hijacked DNA repair proteins and unchained DNA polymerases. Philos Trans R Soc Lond B Biol Sci. 2009; 364:605–611. [PubMed: 19008198]

7. Kawamoto T, et al. Dual roles for DNA polymerase eta in homologous DNA recombination and translesion DNA synthesis. Mol Cell. 2005; 20:793–799. [PubMed: 16337602]

8. McIlwraith MJ, et al. Human DNA Polymerase η Promotes DNA Synthesis from Strand Invasion Intermediates (D-loops) of Homologous Recombination. Mol Cell. 2005; 20:783–792. [PubMed: 16337601]

9. Bugreev DV, Hanaoka F, Mazin AV. Rad54 dissociates homologous recombination intermediates by branch migration. Nat Struct Mol Biol. 2007; 14:746–753. [PubMed: 17660833]

10. Rey L, et al. Human DNA polymerase eta is required for common fragile site stability during unperturbed DNA replication. Mol Cell Biol. 2009; 29:3344–3354. [PubMed: 19380493]

11. Broughton BC, et al. Molecular analysis of mutations in DNA polymerase eta in xeroderma pigmentosum-variant patients. Proc Natl Acad Sci U S A. 2002; 99:815–820. [PubMed: 11773631]

12. Tanioka M, et al. Molecular analysis of DNA polymerase eta gene in Japanese patients diagnosed as xeroderma pigmentosum variant type. J Invest Dermatol. 2007; 127:1745–1751. [PubMed: 17344931]

13. Inui H, et al. Xeroderma pigmentosum-variant patients from America, Europe, and Asia. J Invest Dermatol. 2008; 128:2055–2068. [PubMed: 18368133]

14. Kusumoto R, Masutani C, Shimmyo S, Iwai S, Hanaoka F. DNA binding properties of human DNA polymerase eta: implications for fidelity and polymerase switching of translesion synthesis. Genes Cells. 2004; 9:1139–1150. [PubMed: 15569147]

15. McCulloch SD, et al. Preferential *cis-syn* thymine dimer bypass by DNA polymerase η occurs with biased fidelity. Nature. 2004; 428:97–100. [PubMed: 14999287]

16. Yao J, Dixon K, Carty MP. A single (6-4) photoproduct inhibits plasmid DNA replication in xeroderma pigmentosum variant cell extracts. Environ Mol Mutagen. 2001; 38:19–29. [PubMed: 11473384]

17. Scrima A, et al. Structural basis of UV DNA-damage recognition by the DDB1-DDB2 complex. Cell. 2008; 135:1213–1223. [PubMed: 19109893]

18. Sugasawa K. XPC: its product and biological roles. Adv Exp Med Biol. 2008; 637:47–56. [PubMed: 19181110]

19. Yang W, Woodgate R. What a difference a decade makes: insights into translesion DNA synthesis. Proc Natl Acad Sci U S A. 2007; 104:15591–15598. [PubMed: 17898175]

20. Broyde S, Wang L, Rechkoblit O, Geacintov NE, Patel DJ. Lesion processing: high-fidelity versus lesion-bypass DNA polymerases. Trends Biochem Sci. 2008; 33:209–219. [PubMed: 18407502]

21. Trincao J, et al. Structure of the catalytic core of *S. cerevisiae* DNA polymerase η: implications for translesion DNA synthesis. Mol Cell. 2001; 8:417–426. [PubMed: 11545743]

22. Alt A, et al. Bypass of DNA lesions generated during anticancer treatment with cisplatin by DNA polymerase eta. Science. 2007; 318:967–970. [PubMed: 17991862]

23. Wang L, Broyde S, Zhang Y. Polymerase-tailored variations in the water-mediated and substrate-assisted mechanism for nucleotidyl transfer: insights from a study of T7 DNA polymerase. J Mol Biol. 2009; 389:787–796. [PubMed: 19389406]

24. Ling H, Boudsocq F, Woodgate R, Yang W. Crystal structure of a Y-family DNA polymerase in action: a mechanism for error-prone and lesion-bypass replication. Cell. 2001; 107:91–102. [PubMed: 11595188]

25. Glick E, Vigna KL, Loeb LA. Mutations in human DNA polymerase η motif II alter bypass of DNA lesions. Embo J. 2001; 20:7303–7312. [PubMed: 11743006]

26. Li Y, et al. Nucleotide insertion opposite a cis-syn thymine dimer by a replicative DNA polymerase from bacteriophage T7. Nat Struct Mol Biol. 2004; 11:784–790. [PubMed: 15235589]

27. Ling H, Boudsocq F, Plosky BS, Woodgate R, Yang W. Replication of a cis-syn thymine dimer at atomic resolution. Nature. 2003; 424:1083–1087. [PubMed: 12904819]

28. Park H, et al. Crystal structure of a DNA decamer containing a cis-syn thymine dimer. Proc Natl Acad Sci U S A. 2002; 99:15965–15970. [PubMed: 12456887]

29. Vassylyev DG, et al. Atomic model of a pyrimidine dimer excision repair enzyme complexed with a DNA substrate: structural basis for damaged DNA recognition. Cell. 1995; 83:773–782. [PubMed: 8521494]

30. Min JH, Pavletich NP. Recognition of DNA damage by the Rad4 nucleotide excision repair protein. Nature. 2007; 449:570–575. [PubMed: 17882165]

31. Mees A, et al. Crystal structure of a photolyase bound to a CPD-like DNA lesion after in situ repair. Science. 2004; 306:1789–1793. [PubMed: 15576622]

32. Yang W. Poor base stacking at DNA lesions may initiate recognition by many repair proteins. DNA Repair (Amst). 2006; 5:654–666. [PubMed: 16574501]

33. Lone S, et al. Human DNA polymerase kappa encircles DNA: implications for mismatch extension and lesion bypass. Mol Cell. 2007; 25:601–614. [PubMed: 17317631]

34. Bauer J, et al. A structural gap in Dpo4 supports mutagenic bypass of a major benzo[a]pyrene dG adduct in DNA through template misalignment. Proc Natl Acad Sci U S A. 2007; 104:14905–14910. [PubMed: 17848527]

35. Jia L, Geacintov NE, Broyde S. The N-clasp of human DNA polymerase kappa promotes blockage or error-free bypass of adenine- or guanine-benzo[a]pyrenyl lesions. Nucleic Acids Res. 2008; 36:6571–6584. [PubMed: 18931375]

36. Ling H, Boudsocq F, Woodgate R, Yang W. Snapshots of replication through an abasic lesion; structural basis for base substitutions and frameshifts. Mol Cell. 2004; 13:751–762. [PubMed: 15023344]

37. Wilson RC, Pata JD. Structural insights into the generation of single-base deletions by the Y family DNA polymerase dbh. Mol Cell. 2008; 29:767–779. [PubMed: 18374650]

38. Jarosz DF, Godoy VG, Delaney JC, Essigmann JM, Walker GC. A single amino acid governs enhanced activity of DinB DNA polymerases on damaged templates. Nature. 2006; 439:225–228. [PubMed: 16407906]

39. Lehmann AR, et al. Translesion synthesis: Y-family polymerases and the polymerase switch. DNA Repair (Amst). 2007; 6:891–899. [PubMed: 17363342]

40. Di Lucca J. Variants of the xeroderma pigmentosum variant gene (POLH) are associated with melanoma risk. Eur J Cancer. 2009; 45:3228–3236. [PubMed: 19477635]

41. Bassett E, et al. Efficiency of extension of mismatched primer termini across from cisplatin and oxaliplatin adducts by human DNA polymerases beta and eta in vitro. Biochemistry. 2003; 42:14197–14206. [PubMed: 14640687]

42. Kokoska RJ, McCulloch SD, Kunkel TA. The efficiency and specificity of apurinic/apyrimidinic site bypass by human DNA polymerase eta and Sulfolobus solfataricus Dpo4. J Biol Chem. 2003; 278:50537–50545. [PubMed: 14523013]

43. Kusumoto R, Masutani C, Iwai S, Hanaoka F. Translesion synthesis by human DNA polymerase eta across thymine glycol lesions. Biochemistry. 2002; 41:6090–6099. [PubMed: 11994004]

44. Masutani C, Kusumoto R, Iwai S, Hanaoka F. Mechanisms of accurate translesion synthesis by human DNA polymerase η. EMBO J. 2000; 19:3100–3109. [PubMed: 10856253]

45. Wang F, Yang W. Structural insight into translesion synthesis by DNA Pol II. Cell. 2009; 139:1279–1289. [PubMed: 20064374]

46. McCoy AJ. Solving structures of protein complexes by molecular replacement with Phaser. Acta Crystallogr D Biol Crystallogr. 2007; 63:32–41. [PubMed: 17164524]

47. Hendrickson WA, Horton JR, LeMaster DM. Selenomethionyl proteins produced for analysis by multiwavelength anomalous diffraction (MAD): a vehicle for direct determination of three-dimensional structure. EMBO J. 1990; 9:1665–1672. [PubMed: 2184035]

48. Brünger AT, et al. Crystallography and NMR system: a new software suite for macromolecular structure determination. Acta Crystallogr. 1998; D54:905–921.

49. Emsley P, Lohkamp B, Scott WG, Cowtan K. Features and Development of Coot. Acta Crystallographica Section D. 2010; 66:486–501.
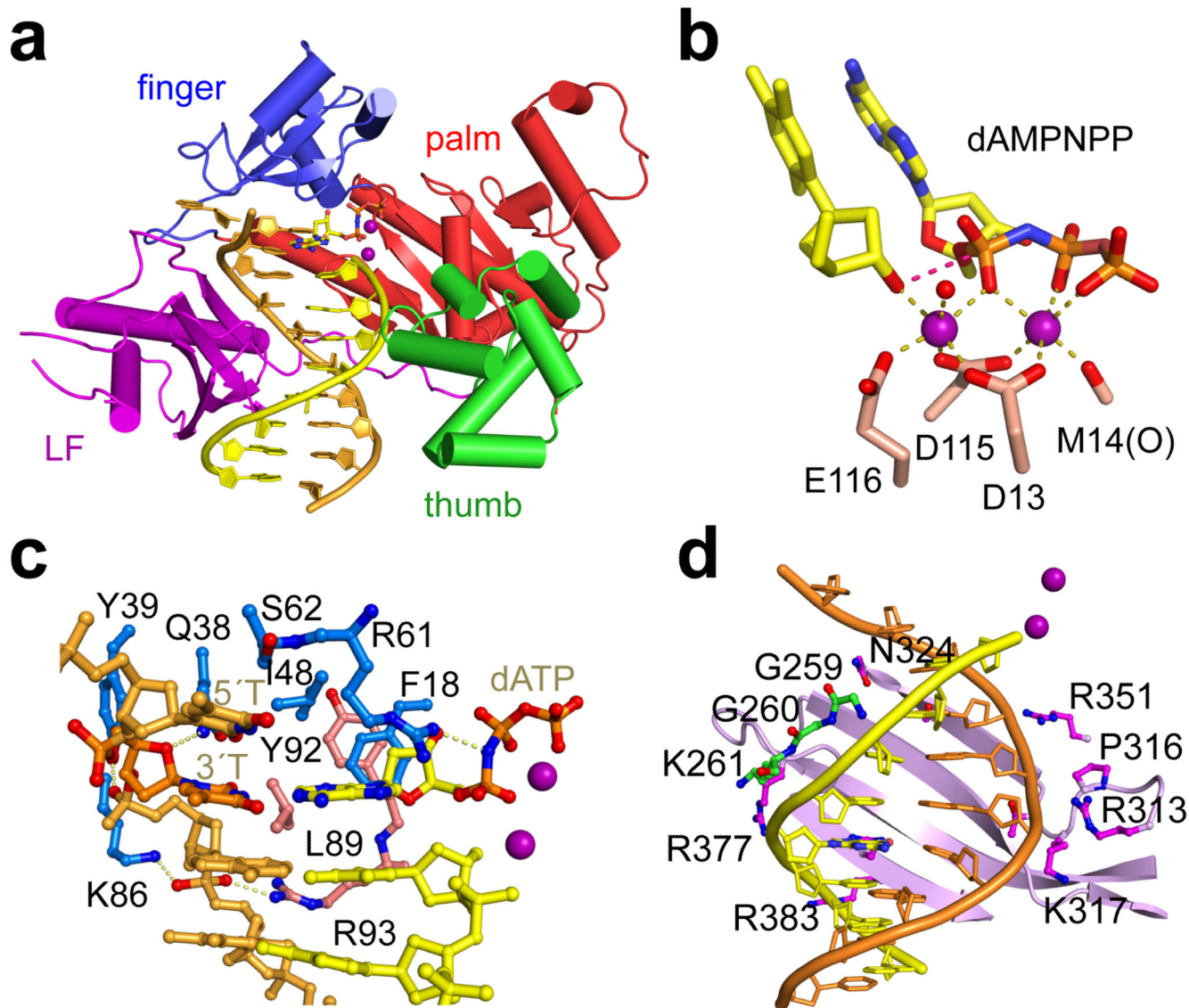
Figure 1.

Structure of hPol η. **a.** The ternary complex of hPol η with a normal DNA. Protein domains are shown in distinct colors and labeled. The DNA template is colored orange and the primer yellow. Oxygen and nitrogen atoms are colored red and blue, respectively. dAMPNPP is shown as stick-and-balls, and Mg^{2+} as purple spheres. All structural figures were made using PyMOL (www.pymol.org). **b.** The active site. Mg^{2+} coordination is indicated by pale yellow dashed lines. The 3′-OH of the primer strand is 3.2Å from the α-phosphate as indicated by the red dashed line. **c.** hPol η-DNA interactions around the active site. Protein side chains from the finger and palm domain are shown as light blue and pink sticks, respectively. **d.** Interactions with the upstream DNA. LF (shown as light purple ribbon diagram) contacts both template and primer, and the thumb domain (shown in green) only makes 3–4 hydrogen bonds with the primer strand. Side chains that make DNA contacts are highlighted in sticks and labeled.
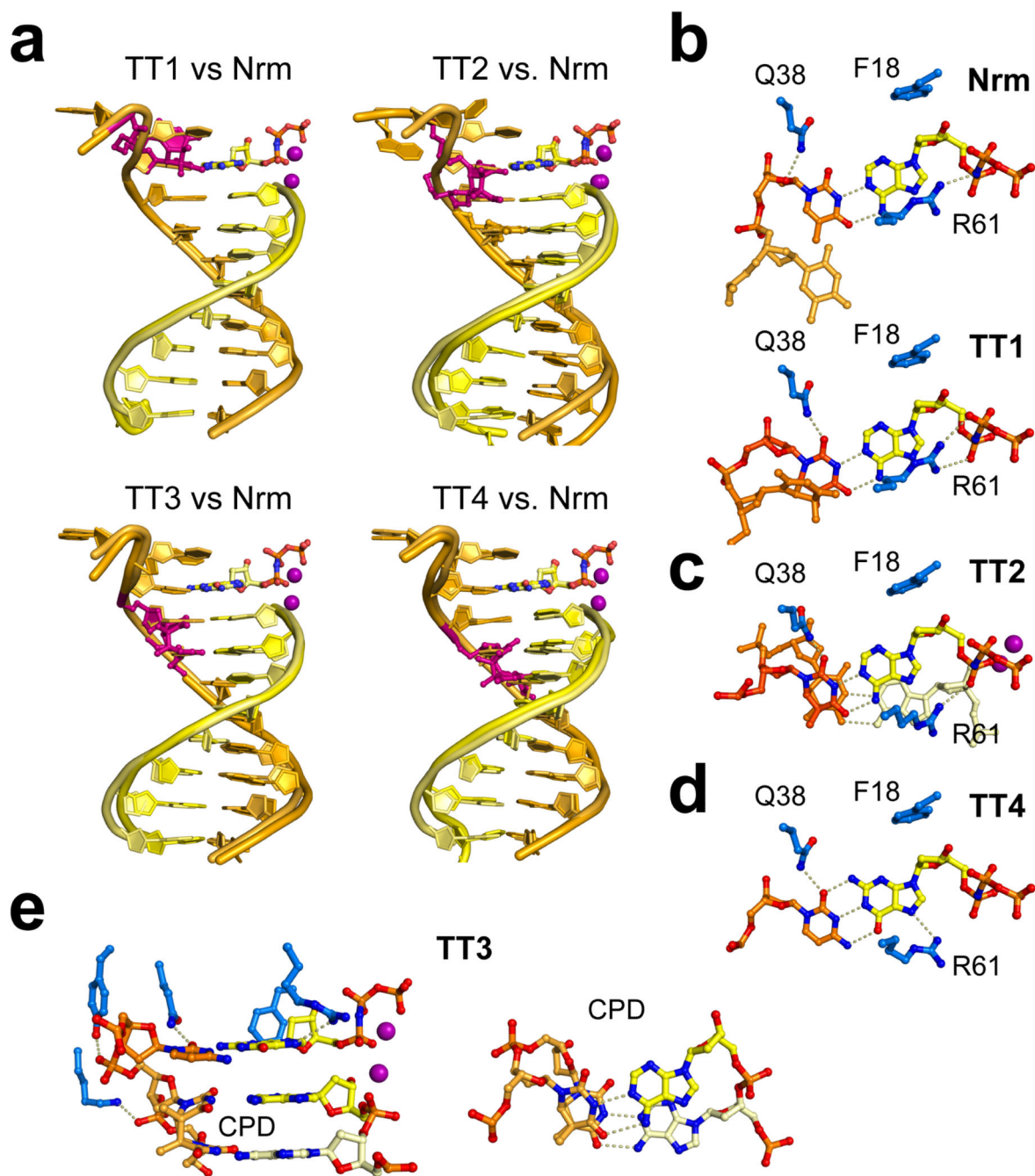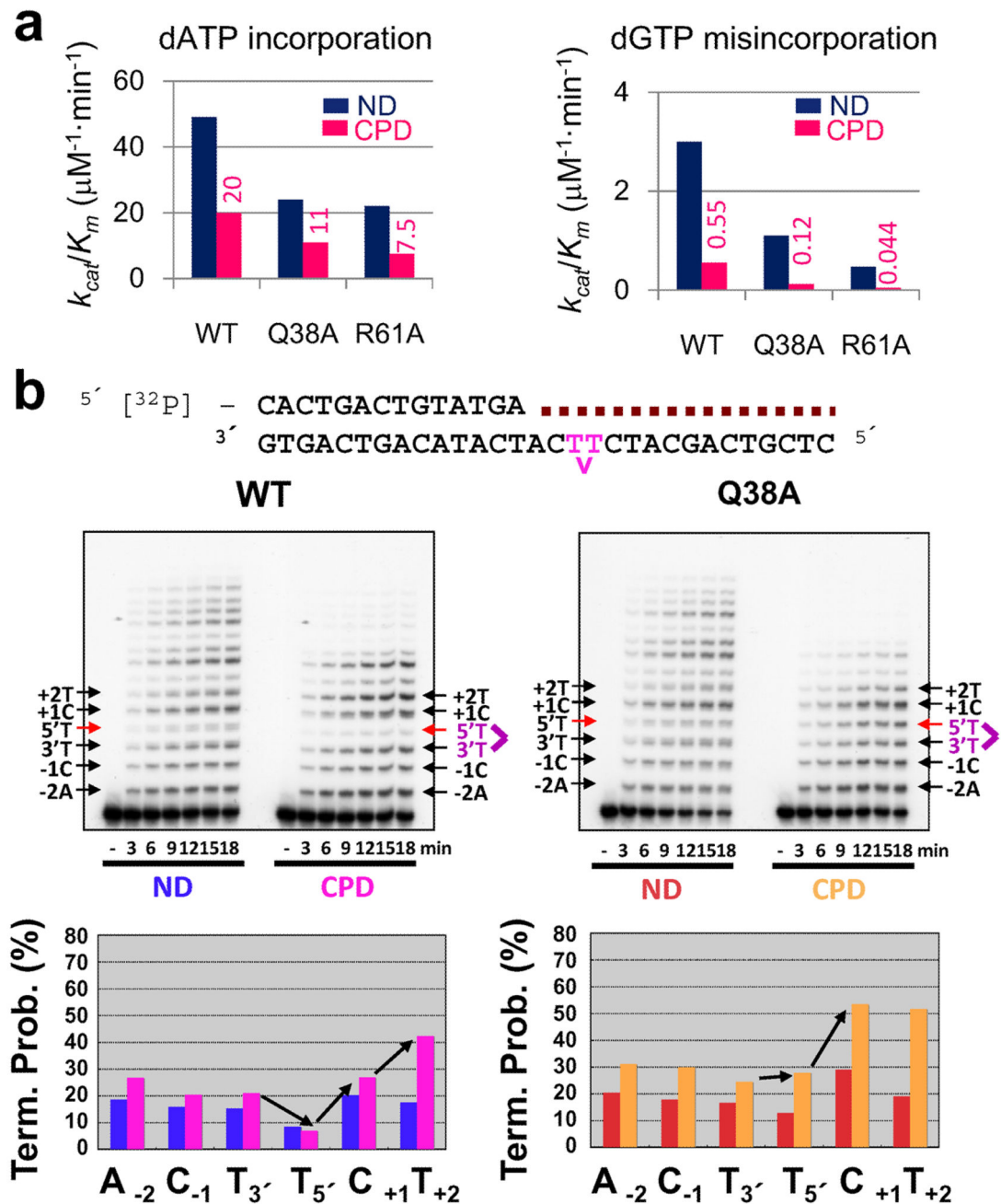
Figure 2.
Structures of lesion DNAs. **a**. Overlay of TT1, TT2, TT3 and TT4 DNA with the DNA in Nrm (undamaged). CPDs are shown as red sticks. DNA and Mg^{2+} are colored as in Fig. 1. **b**–**d**. The replicating base pairs in four ternary complexes (highly similar in TT3 and TT4) are each shown with hPol η residues that contact the bases and deoxyribose. Hydrogen bonds are shown as dashed lines. **e**. CPD in TT3 and TT4 forms WC-like hydrogen bonds but cannot base stack with neighboring nucleotides.

Figure 3.
Functional analyses of Q38A and R61A Pol η. **a**. Efficiencies (k_{cat}/K_M) of WT and two mutants in correct and incorrect nucleotide incorporation on normal (ND) and CPD DNA. These values are derived from Supplementary Table 3. **b**. CPD-bypass by WT (left) and Q38A mutant Pol η (right). The DNA sequence for primer extension assays is shown. Magenta colored TT represents the CPD. The same DNA template with a 2 nt longer primer was used for the kinetic assay shown in Fig. 3a. Reactions were carried out at a substrate:enzyme molar ratio of 100:1 for the indicated incubation time. Termination

probabilities ($[I_n] / \Sigma_{n\text{-end}}[I]$, where I_n is band intensity at the nth position) on normal (ND) and CPD DNA are plotted below.
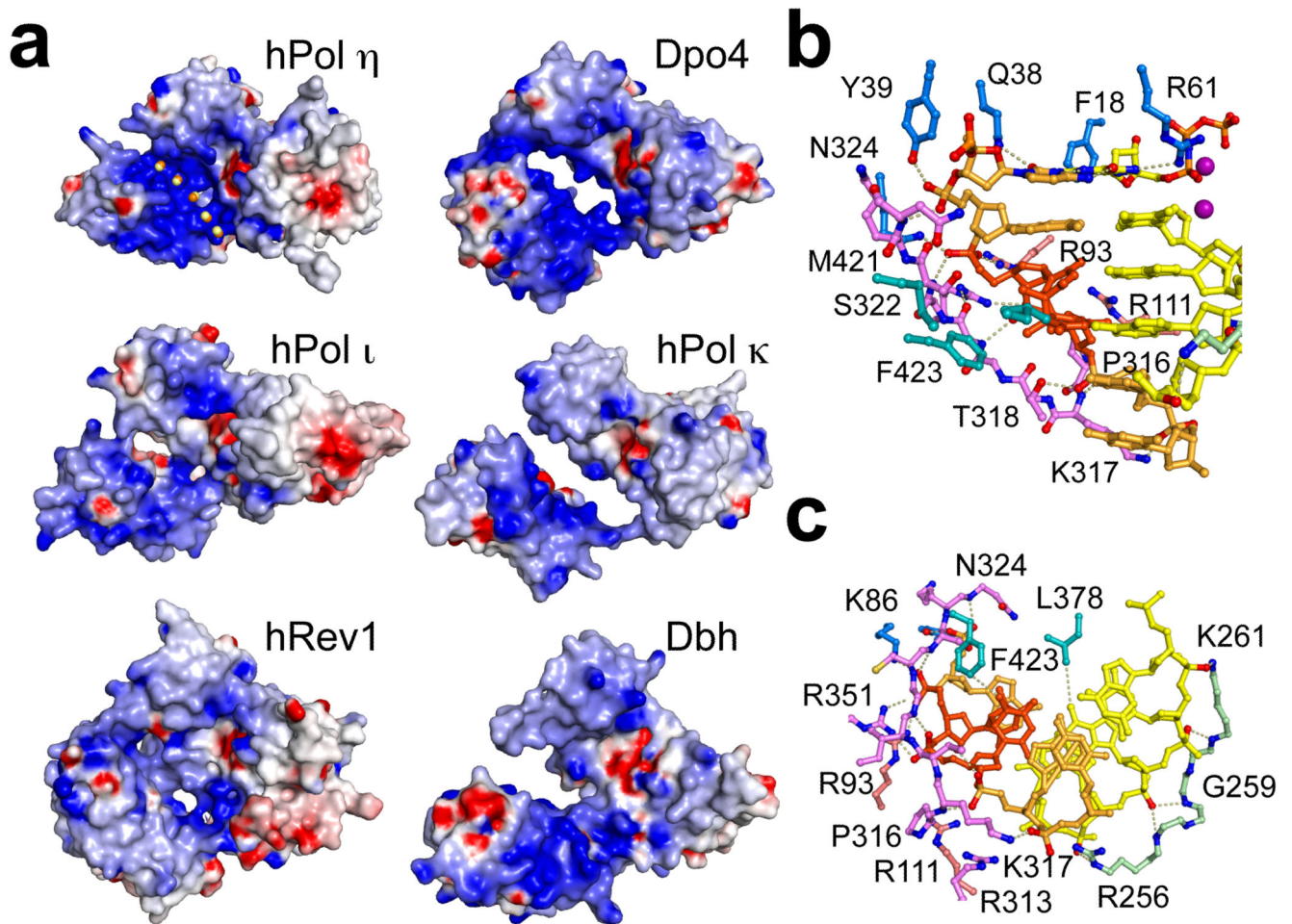
Figure 4.
hPol η is a molecular splint. **a**. The DNA binding surfaces of various Y-family polymerases are shown with electrostatic potentials. Blue and red represent the positive and negative charge potential at the + and − 10 kT/e scale, respectively. The thumb domain in all cases and the N-clasp of Polκ are removed for clarity. Five phosphorus atoms at position -1 to -5 in the hPol η Nrm (yellow) and TT4 (orange) structures are also shown. **b**. The extensive interactions between hPolη and the template strand in TT4 (as an example) are shown. Hydrogen bonds are indicated by dashed lines. The finger and LF domains are colored in light purple and light green. Two residues forming hydrophobic interactions with the CPD bases are shown in teal. **c**. A view approximately 90° from **b**. Detailed hPol η-DNA interactions are shown in Supplementary Fig. 9.
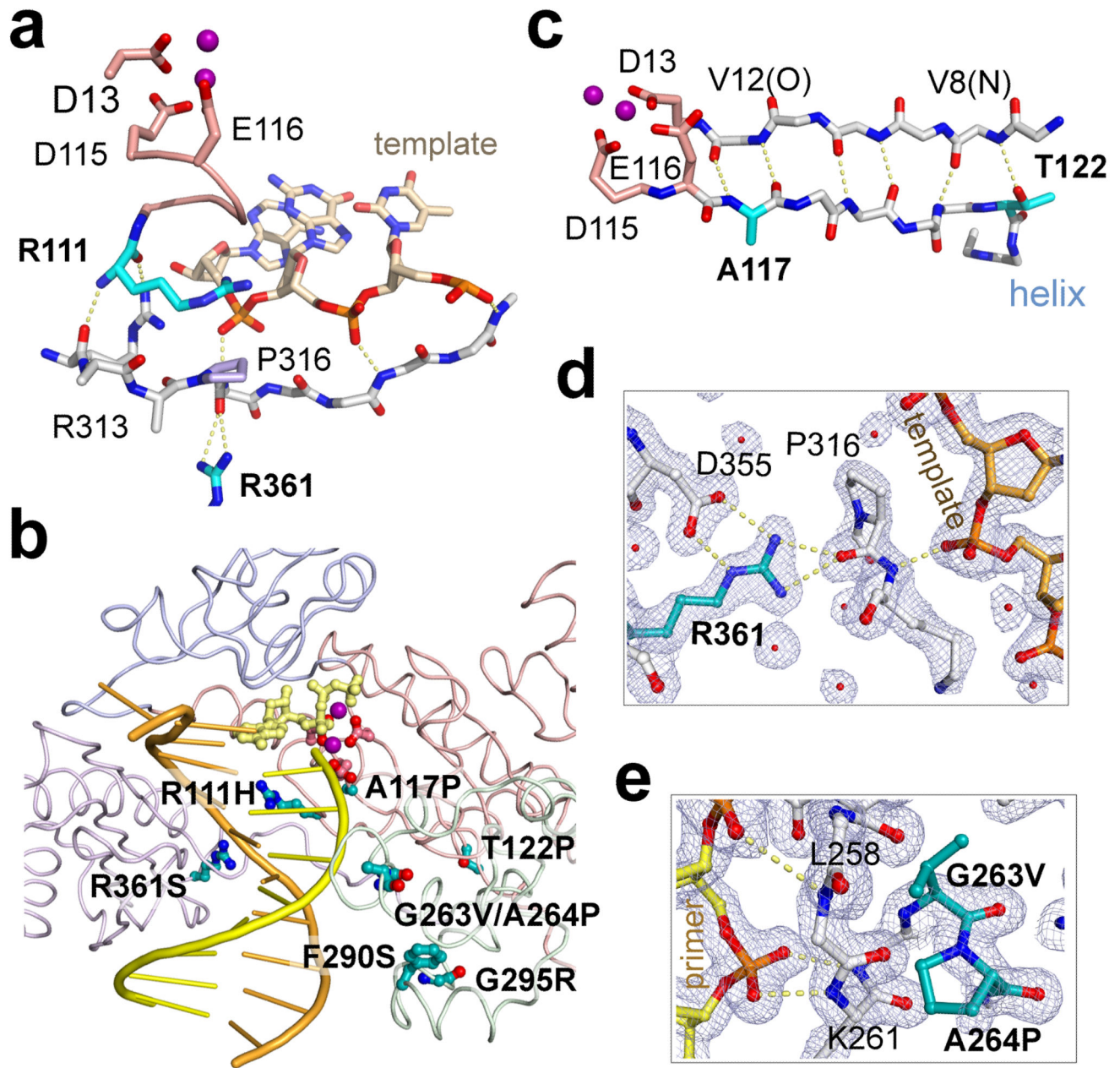
Figure 5.
XPV mutations. **a**. R111 contacts DNA template and stacks with P316 of LF. **b**. Mapping of 8 missense XPV mutations. The protein is represented by the Cα trace, DNA as tube-and-ladders, and the altered residues are shown as cyan ball-and-sticks. **c**. Local interactions of A117 and T122 and their relation to the active site. Most side chains are removed for clarity. **d**. R361 supports P316 and the β strand that forms an extensive hydrogen-bond network with the DNA template. **e**. G263 and A264 are adjacent to the thumb-DNA primer interface. G263V and A264P substitutions would clash with L258 and K261. Electron densities are shown as meshes in panels **c** and **e**.